Article

Effect of MoSi$_2$-Si$_3$N$_4$/SiC Multi-Layer Coating on the Oxidation Resistance of Carbon/Carbon Composites above 1770 K

Imran Abbas [1], Yanxiang Wang [1], Hassan Elahi [2,*] , Muhammad Ali Siddiqui [3], Mudaser Ullah [4] and Faisal Qayyum [5]

[1] Carbon Fiber Engineering Research Center, Faculty of Materials Science, Shandong University, Jinan 250061, China; engr.imran514@outlook.com (I.A.); wyx079@sdu.edu.cn (Y.W.)

[2] Department of Mechanical and Aerospace Engineering, Sapienza University of Rome, 00184 Rome, Italy

[3] Institute of Metal Research, Chinese academy of sciences, 72 Wenhua Road, Shenyang 110016, China; mueatali@yahoo.com

[4] Department of Mechanical Engineering, CET, University of Sargodha, Sargodha 40100, Pakistan; mudaser_me150@yahoo.com

[5] Institutfür Metallformung, Technische Universität Bergakademie Freiberg, D-09599 Freiberg, Germany; faisal.qayyum@student.tu-freiberg.de

* Correspondence: hassan.elahi@uniroma1.it

check for
updates

Abstract: To improve the oxidation resistance of carbon/carbon composites at high temperatures (>1770 K), they were coated with MoSi$_2$-Si$_3$N$_4$/SiC. The slurry and pack cementation methods were adopted to deposit the inner SiC layer and outer MoSi$_2$-Si$_3$N$_4$ layer. The phase composition, microstructure, and elemental distributions in the coating were analyzed using SEM, XRD, EDS, and Raman spectroscopy. Oxidation tests show that the deposited multi-layer coating can protect the carbon/carbon matrix from oxidation at high temperatures (>1770 K) for 150h and that the coating can withstand 40 thermal cycles between 1773 and 300 K. It is observed that Si$_3$N$_4$ assists in the formation of a dense SiO$_2$ layer at a high temperature, which plays a vital role in increasing the thermal cyclic and oxidation resistance of the coating itself. The weight loss of coated carbon/carbon composite is attributed to the formation of micro-cracks and diffusion of SiO$_2$, MoO$_3$, and N$_2$ out of the material at high temperatures.

Keywords: carbon/carbon composites; multi-phase coatings; oxidation resistance; thermal cycling

1. Introduction

For aggressive service environments in the nuclear and aerospace industry, carbon/carbon composites are candidate structural materials due to their attractive properties such as a high strength-to-weight ratio, thermal cyclic oxidation resistance, strength retention, and a low thermal expansion coefficient [1–5]. However, these composites exhibit limitations such as susceptibility to oxidation beyond 773 K and strength loss upon exposure to high temperatures. This makes them highly unfavorable for specific high-temperature applications [6–8]. It was shown by previous researchers that carbon/carbon composites could be protected against oxidation at high temperatures by the application of anti-oxidizing coatings [9].

In multi-layered coatings, MoSi$_2$ is used as an outer layer, while SiC forms the inner buffer layer. The peripheral multi-layer coating containing MoSi$_2$ exhibits a superior oxidation-resistant capability for carbon/carbon composites at 1500–1600 °C [10]. However, due to the mismatch of the thermal expansion coefficient between the SiC bonding layer and the MoSi$_2$ outer coating, micro-cracks

in the $MoSi_2$ appear at extended high-temperature (i.e., 800–1000 °C) exposure [11–14]. Therefore, the protective temperature range of coatings containing $MoSi_2$ is constricted; this limits the structural and high-temperature applications of such materials. The coefficient of thermal expansion (CTE) of $MoSi_2$ (~8.1×10^{-6}/K) is higher than that of carbon/carbon composites (~1.0×10^{-6}/K). Therefore, the mismatch between the CTEs of the outer $MoSi_2$ layer and the inner SiC-coated carbon/carbon matrix causes the degradation of the coating under thermal cycling and ultimately lowers the coating durability [15,16].

$MoSi_2$ coating at a temperature range of 400–600 °C efficiently reacts with oxygen to form MoO_3 and SiO_2. These oxides result in the considerable volume expansion of the $MoSi_2$ matrix, which results in the disintegration of bulk $MoSi_2$ into powders and causes catastrophic failure of the coating [17]. This is called the "pest phenomenon" and is another primary reason for coating failure. In addition, $MoSi_2$ is a low toughness material which limits its industrial application even at ambient temperature [18].

Earlier reports have suggested that the addition of Si_3N_4 to $MoSi_2$ can minimize the coefficient of thermal expansion (CTE) mismatch between the outer $MoSi_2$ and inner SiC coatings. Si_3N_4 exhibits high flexural strength and excellent compatibility with $MoSi_2$ and SiC due to better mixing with these compounds. It also exhibits a reasonable resistance to creep, isothermal oxidation, and cyclic thermal oxidation [19]. The $MoSi_2$-Si_3N_4 coating exhibits excellent oxidation resistance with minute weight loss. At high temperature, $MoSi_2$-Si_3N_4 forms a dense glassy SiO_2 film on the coating surface. Owing to its low oxygen-diffusion coefficient, the SiO_2 film serves as an oxygen diffusion barrier and efficiently protects carbon/carbon composites from oxidation at 1773 K [20,21]. Due to good fluidity at high temperatures, SiO_2 can seal all the micro-cracks formed during the volatilization of MoO_3, CO_2, and N_2 [22]. Furthermore, the addition of Si_3N_4 provides better refractory and some oxidation-resistant properties, which decrease the possibility of pest disintegration of $MoSi_2$. Huang et al. [23] prepared a $MoSi_2$/Si_3N_4 coating on Mo substrate and described the effect of the Si_3N_4 content on the microstructure and antioxidant properties of multi-layer coatings.

In this study, coatings composed of a SiC bonding layer and a $MoSi_2$-Si_3N_4 outer layer were prepared by a simple and low-cost slurry method. The phase composition, microstructure, and oxidation resistance of the above multi-layer coatings at 1773 K in the air were investigated in detail.

2. Experimental Procedure

2.1. Coating Preparation

Small specimens ($10 \times 10 \times 10$ mm^3) of carbon/carbon composite (Shandong Weiji Carbon Technology Co. Ltd., Jinan, China) with a density of 1.79g/cm^3 used as substrates were cut from thin bulk sheet. The carbon/carbon composite used in this study was carbon fiber-strengthened graphite. The surface area of the samples was increased by abrading them with commercially available rough SiC papers. To remove any remaining debris and moisture, the samples were cleaned ultrasonically with distilled water and dried in an oven at 100 °C for 2 h.

The powder compositions used were Si 75 wt%, graphite 20 wt%, and Al_2O_3 5 wt% respectively. All the powders used were lab-grade and had a purity ≥ 99% with particle size ranging between 1–10 μm. SiC inner coatings were applied to the specimens by the pack-cementation method. The carbon/carbon composites and pack mixtures were put in a graphite crucible and heated at 1873 K for 2 h in an argon atmosphere to form the SiC coating. After the completion of inner coating, the SiC-coated specimens were cleaned ultrasonically and dried in an oven at 100 °C for 2 h.

The liquid slurry mixture method was adopted for applying the outer coating of $MoSi_2$-Si_3N_4 over the already applied inner SiC coating. High-purity $MoSi_2$ and Si_3N_4 powders supplied by Turnnano Ltd., Henan, China) were used. The $MoSi_2$ and Si_3N_4 powders were mixed in 10mL aqueous solution of H-PSO, and a homogenous slurry solution was prepared. The SiC-coated carbon/carbon specimens were put in a slurry mixture of $MoSi_2$ and Si_3N_4. The as-coated specimens were put in a

graphite crucible and heated up to 2073 K for two hours in the nitrogen atmosphere to apply the outer $MoSi_2$-Si_3N_4 coating on the samples.

The slurry method was preferred over others due to its compositional flexibility, ease of processing, and low cost. Also, it is known that the coating deposited via the slurry method exhibits reasonable resistance to oxidation and thermal cyclic oxidation [11]. The $MoSi_2$-SiC and $MoSi_2$-Si_3N_4/SiC coatings were prepared using a similar approach to elucidate the effect of Si_3N_4 addition on the oxidation resistance of the multi-layer coatings.

2.2. Oxidation Test

Isothermal oxidation tests on the $MoSi_2$-Si_3N_4/SiC multi-layer coated carbon/carbon specimens were performed in a corundum tube furnace at 1773 K for 150 h. After every 10 h to a maximum time of 150 h, the samples were taken out of the furnace directly and cooled to room temperature in air. The weight loss of each specimen at room temperature was measured with an electronic balance with a sensitivity of ±0.1 mg. The percentage weight loss (wt%) was calculated using Equation (1), where m_0 and m_1 are the weights of specimens before and after the oxidation test, respectively.

$$\text{wt\%} = \frac{m_0 - m_1}{m_0} \times 100\%$$

(1)

The thermal cyclic oxidation resistance of the $MoSi_2$-Si_3N_4/SiC multi-layer coating was investigated by conducting a test between 1773 K and room temperature. In this test, the coated carbon/carbon specimens were heated at 1773 K for 10 min, removed from the furnace, and air-cooled to room temperature for each cycle. The testing was carried out in 40 cycles.

2.3. Characterization of the Coatings

The morphology of the $MoSi_2$-Si_3N_4/SiC multi-layer coating before and after the oxidation test was analyzed using a scanning electron microscope (SEM), equipped with an energy dispersive spectroscope (EDS). Raman spectroscopy (LabRam-1B, 633nm line of the He-Ne laser) was used to identify the chemical composition and phase transformation. An X-ray diffraction (XRD) technique was used for the crystallographic characterization of the coating before and after the oxidation test.

To analyze the elemental distribution along with the depth of the coated samples, they were sectioned using a power cutter and were then ground and polished to prepare the surface perpendicular to the top coating surface. These samples were then analyzed using the same characterization techniques stated earlier in this section.

3. Results and Discussion

3.1. Microstructure of Coating before the Oxidation Test

The XRD pattern of the as-coated inner SiC layer is shown in Figure 1a. Three significant peaks at $2\theta \approx 35.6°$, $60.0°$, and $71.7°$ correspond to the (111), (220), and (311) crystalline planes of β-SiC, indicating the formation of the β-SiC crystalline plane during the pack cementation process. The low-intensity peak at $2\theta \approx 33.6°$ indicates the existence of stacking faults (SF) in the β-SiC coating. The stacking faults might be induced due to the thermal stresses produced in the coating process [24].
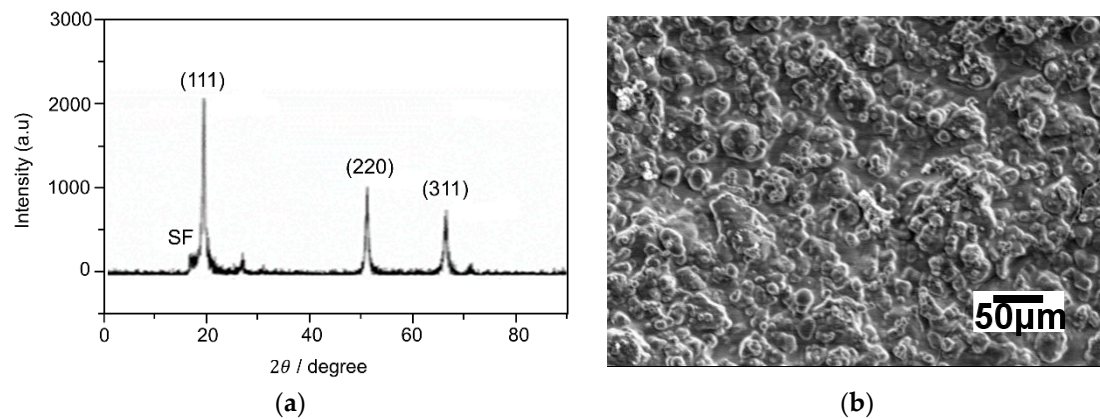
Figure 1. Structure of the inner SiC coating: (**a**) XRD pattern; (**b**) surface SEM image.

Figure 1b shows the surface microstructure of the as-coated inner SiC layer. Figure 2 shows the XRD analysis of the as-coated specimen, i.e., the $MoSi_2$-Si_3N_4/SiC-coated carbon/carbon specimen before the oxidation test. $MoSi_2$, Si_3N_4, and SiC phases are apparent. The more vigorous peak intensity of the $MoSi_2$ phase in Figure 2 indicates that it is relatively more abundant in the slurry.
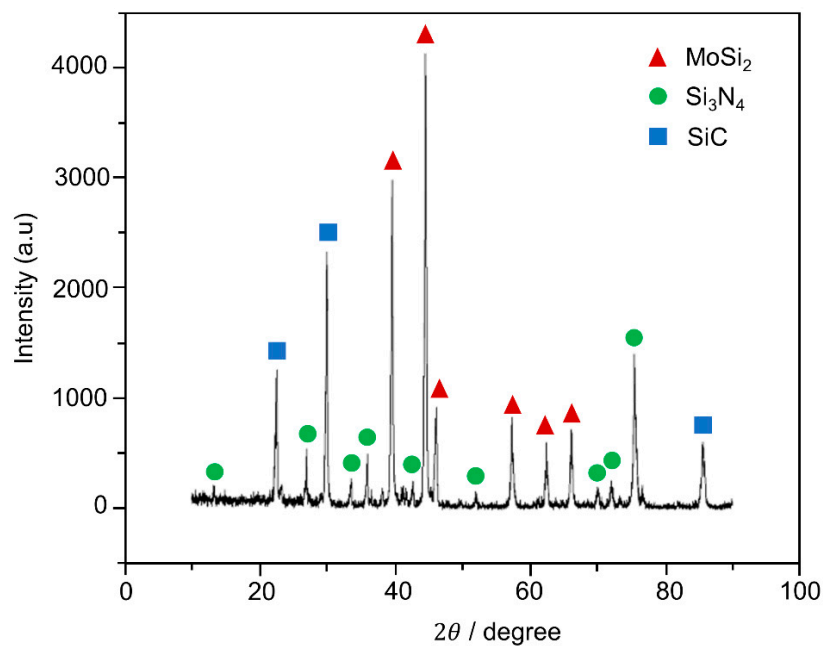
Figure 2. XRD pattern of $MoSi_2$-Si_3N_4/SiC coated carbon/carbon specimen before the oxidation test.

Figure 3a shows the surface microstructure of the as-coated $MoSi_2$-Si_3N_4 outer layer before the oxidation test. The surface of the coating has no micro-cracks, indicating that the as-prepared coating is dense and homogeneous. In Figure 3b, the EDS pattern of the area marked with the red square in Figure 3a clearly shows that the smooth area of the as-coated $MoSi_2$-Si_3N_4 is composed of the elements Si, N, and Mo.
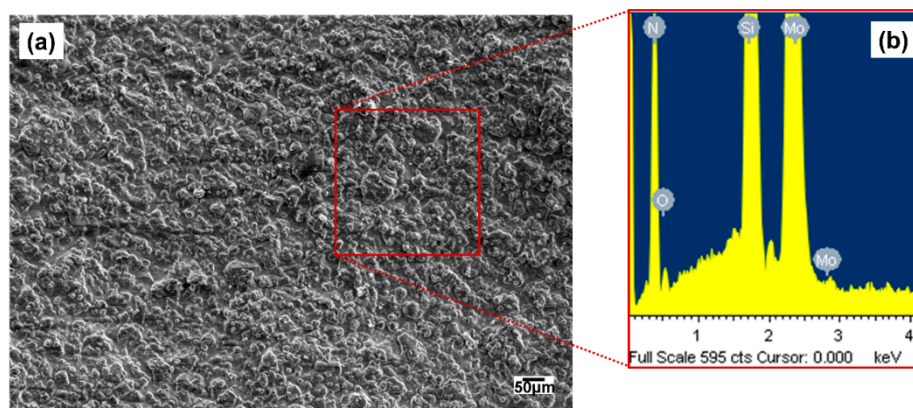
Figure 3. Surface of the as-coated $MoSi_2$-Si_3N_4 outer layer: (**a**) SEM image; (**b**) EDS pattern corresponding to the marked red square in Figure 3a.

Figure 4 shows an overlay of element line scanning over the SEM image of the cross-section of $MoSi_2$-Si_3N_4/SiC coated C/C composite before the oxidation test. The multi-layer coating has an average thickness of 195 ± 3 μm. It can be observed from the line scan that the as-prepared coating is composed of a $MoSi_2$-Si_3N_4 outer layer, SiC inner layer, and SiC transition layer, of thicknesses 40 ± 5, 61 ± 2, and 93 ± 2 μm, respectively. The SiC transition layer, formed possibly due to the infiltration of Si into the carbon/carbon substrate at high temperature, increases the oxidation and thermal cyclic oxidation resistance of the coating. The lack of voids between the outer and inner coating layers in Figure 4 indicate two things:

1. An increase in the interfacial bonding strength of the coating [25];
2. A reduction in the thermal mismatch of the expansion between the coatings and the C/C substrate.
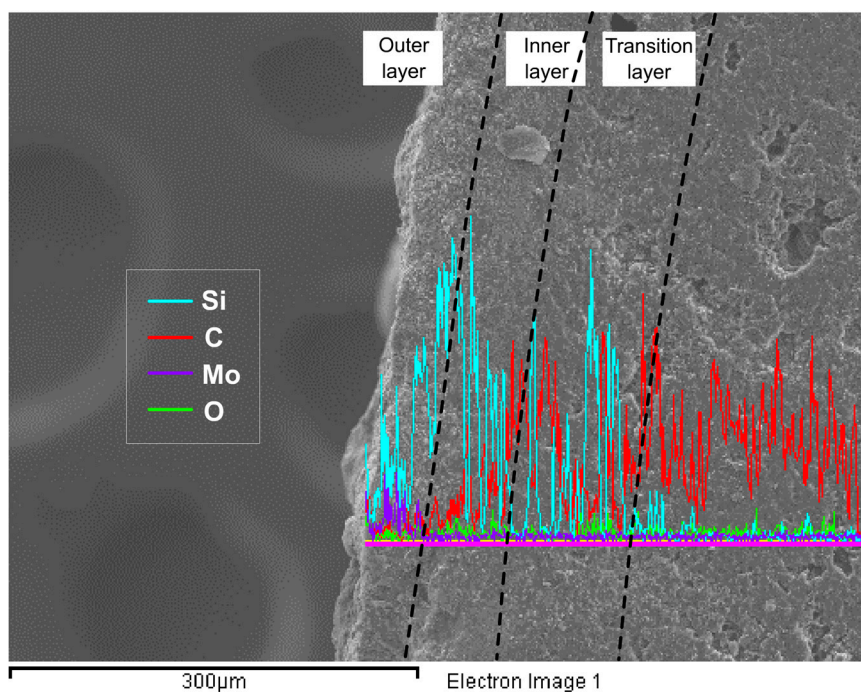
Figure 4. Line scans of the cross-section of C/C composite coated with $MoSi_2$-Si_3N_4/SiC.

3.2. Microstructure of Coating Post-Oxidation Test: Oxidation Resistance Evaluation

Figure 5 shows the XRD spectrum of the $MoSi_2$-Si_3N_4/SiC coating after the oxidation test at 1773 K. It is clear that the oxidation test resulted in the formation of several new phases. The $MoSi_2$ phase of

the MoSi$_2$-Si$_3$N$_4$/SiC coating has undergone complete transformation, producing some new phases, SiO$_2$, Mo$_5$Si$_3$, and MoO$_3$. The appearance of large fractions of Si-based new phases indicates that MoSi$_2$ is completely oxidized. The partial oxidation of Si$_3$N$_4$ at oxidation temperature has resulted in the formation of the Si$_2$N$_2$O phase that is in accordance with the XRD pattern [26]. The possible reactions are as follows.

$$\text{SiC (s)} + 2\text{O}_2\text{(g)} \rightarrow \text{SiO}_2 + \text{CO}_2 \text{ (g)} \tag{2}$$

$$5\text{MoSi}_2 \text{ (s)} + 7\text{O}_2 \text{ (g)} \rightarrow \text{Mo}_5\text{Si}_3 \text{ (s)} + 7\text{SiO}_2 \text{ (s)} \tag{3}$$

$$2\text{Mo}_5\text{Si}_3 \text{ (s)} + 21\text{O}_2 \text{ (g)} \rightarrow 10\text{MoO}_3 \text{ (g)} + 6\text{SiO}_2 \text{ (s)} \tag{4}$$

$$2\text{MoSi}_2 \text{ (s)} + 7\text{O}_2 \text{ (g)} \rightarrow 4\text{SiO}_2 \text{ (s)} + 2\text{MoO}_3 \text{ (g)} \tag{5}$$

$$\text{Si}_3\text{N}_4 \text{ (s)} + 3\text{O}_2 \text{ (g)} \rightarrow 3\text{SiO}_2 \text{ (s)} + 2\text{N}_2 \text{ (g)} \tag{6}$$

$$\text{Si}_3\text{N}_4 \text{ (s)} + \text{SiO}_2 \text{ (s)} \rightarrow 2\text{Si}_2\text{N}_2\text{O (s)} \tag{7}$$
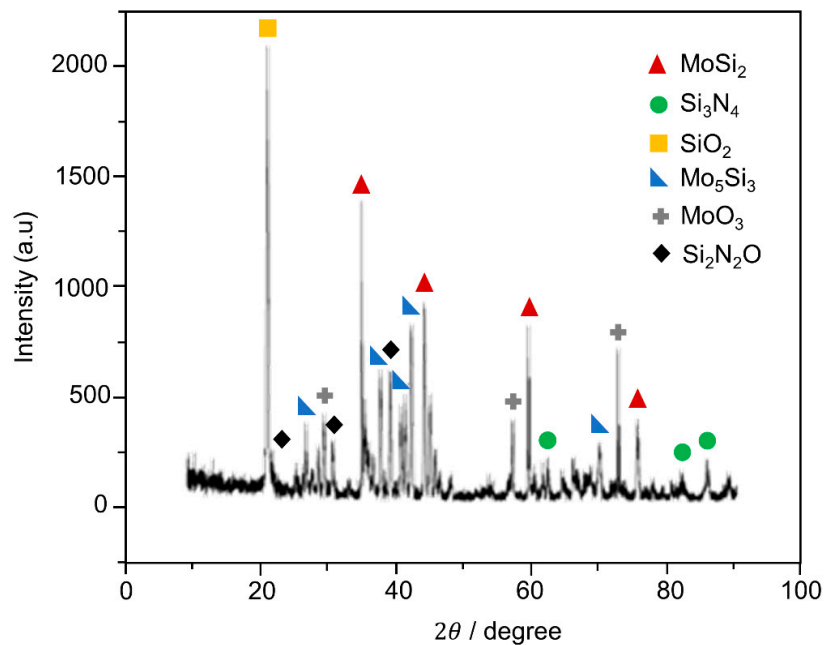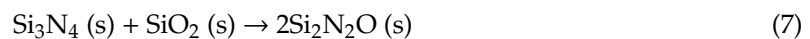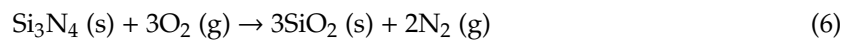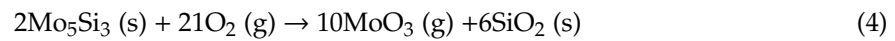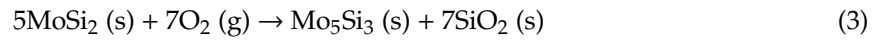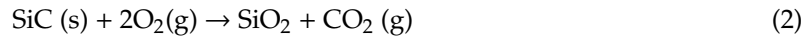
Figure 5. XRD pattern of MoSi$_2$-Si$_3$N$_4$/SiC-coated C/C composites after oxidation at 1773 K.

Mo$_5$Si$_3$ and SiO$_2$ play an important role in increasing the oxidation resistance of the coating. The Mo$_5$Si$_3$ phase increases the coating flexural strength and the coating-substrate compatibility and enhances the creep strength [27]. The SiO$_2$ phase, owing to its inherent low viscosity, good fluidity and low oxygen permeability, serves as a barrier against oxygen attack. In Figure 6, the Raman spectroscopy result also confirms the formation of SiO$_2$ in the MoSi$_2$-Si$_3$N$_4$ coating after oxidation at 1773 K. It can be found that the peak with wave number of 228 and 414 cm^{-1} is the crystallite while the wave number of 1034 cm^{-1} is the amorphous silica, which is accordance with the XRD result.
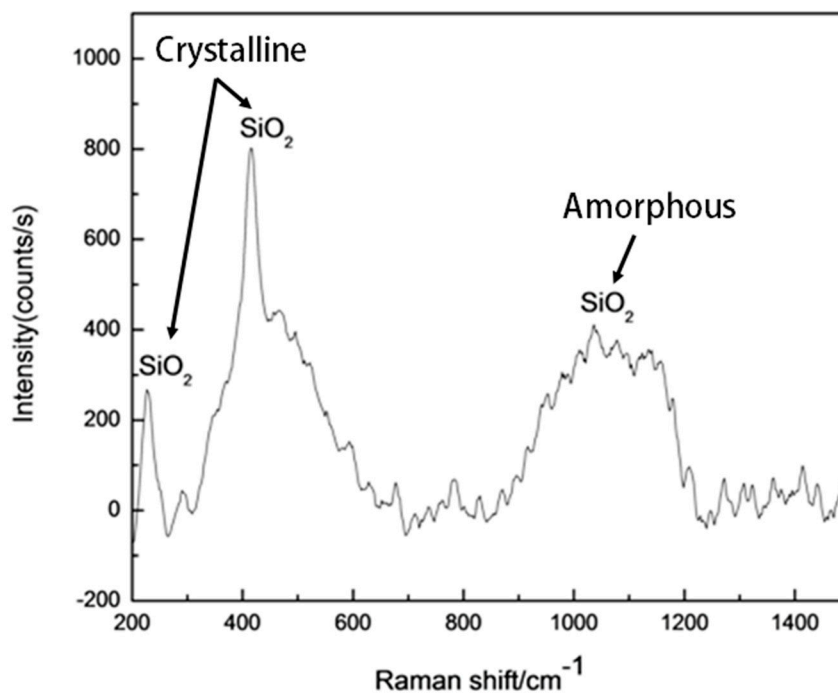
Figure 6. Raman spectrum of the $MoSi_2$-Si_3N_4/SiC coating after oxidation at 1773 K for 150 h [26].

The effect of Si_3N_4 on the oxidation resistance of the multi-layer coating was investigated from the microstructure analysis and weight loss of the coatings constituting the $MoSi_2$ and $MoSi_2$-Si_3N_4 outer layers. Figure 7a shows the microstructure of the $MoSi_2$ surface of the $MoSi_2$/SiC multi-layer coating after the oxidation test. The incomplete formation of silica (SiO_2) was due to the non-uniform agglomeration of $MoSi_2$ particles in the brushing process [28]. These particles degraded the surface of the coating and gradually reduced its oxidation resistance. As a result, some deep cracks occurred and propagated through the randomly deposited $MoSi_2$.

Figure 7b shows the SEM micrograph of the cross-section of $MoSi_2$/SiC multi-layer-coated carbon/carbon composites. The cross-section is rough, porous, and oxidized. This is because of the large CTE difference between SiC and $MoSi_2$, leading to the incomplete formation of SiO_2 and pore/cavity formation [25,29]. These pores provide the diffusion channel for oxygen that penetrates the substrate and causes the failure of the coating. It is also noteworthy that the infiltration of oxygen via the cavities would reduce the thickness of the coating. Therefore, the porous morphology of the $MoSi_2$/SiC coating is detrimental for its oxidation resistance.

Figure 7c shows the microstructure of the outer surface of the $MoSi_2$-Si_3N_4/SiC coating after the oxidation test at 1773 K. A dense glassy SiO_2 layer on the surface is evident, which prevents the carbon/carbon matrix from oxygen penetration and protects the coating from oxidation. This makes the $MoSi_2$-Si_3N_4/SiC coating oxidation-resistant and an ideal choice for high-temperature applications.

In Figure 7d, the cross-sectional morphology of the post-oxidation tested $MoSi_2$-Si_3N_4/SiC coating exhibits excellent compatibility between the coating and the substrate, which is responsible for the high bonding and flexural strengths of the coating in high-temperature environments [30,31]. Furthermore, the absence of voids/holes at the coating–substrate interface indicates that the coating is resistant to high-temperature rupture. In addition, Si_3N_4 forms a suitable combination with $MoSi_2$ in the slurry, which helps to minimize the CTE difference between the outer $MoSi_2$-Si_3N_4 layer and the inner SiC-coated carbon/carbon substrate. Therefore, Si_3N_4 plays a vital role in increasing the oxidation protective ability of outer coatings at high temperatures [32]. The formation of microdefects (i.e., microcracks and micropores) is due to the volatilization of MoO_3. From experimental observations, these pores are far from detrimental to the coating and can be cured by the glassy SiO_2 layer at high temperatures.
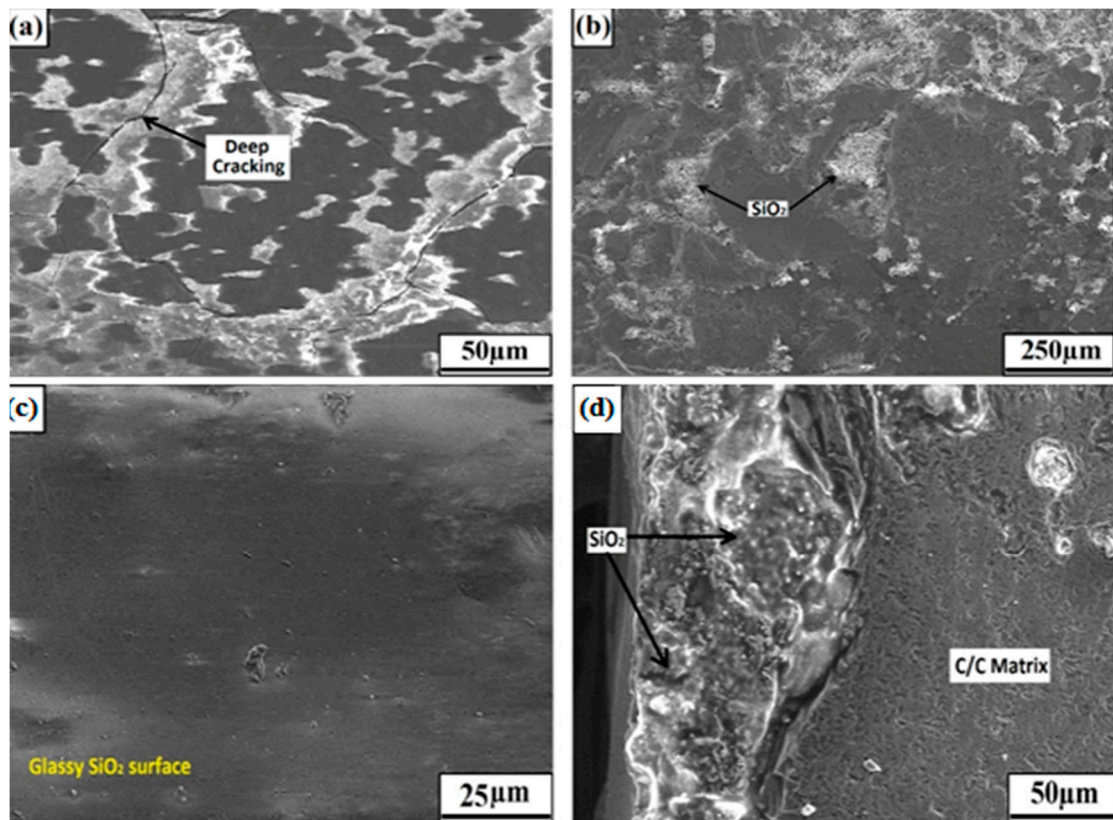
Figure 7. SEM image of MoSi$_2$/SiC coating after oxidation at 1773 K: (**a**) surface, (**b**) cross-section; SEM image of MoSi$_2$-Si$_3$N$_4$/SiC coating after oxidation at 1773 K: (**c**) surface, (**d**) cross-section.

Figure 8 shows a comparison of weight losses for the two coatings, with and without Si$_3$N$_4$, after the oxidation test at 1773 K. The MoSi$_2$-Si$_3$N$_4$/SiC coating experienced a weight loss of 0.9% after 150 h of oxidation treatment while the MoSi$_2$/SiC coating suffered a relatively high weight loss of 4.0% even after 90 h of oxidation.
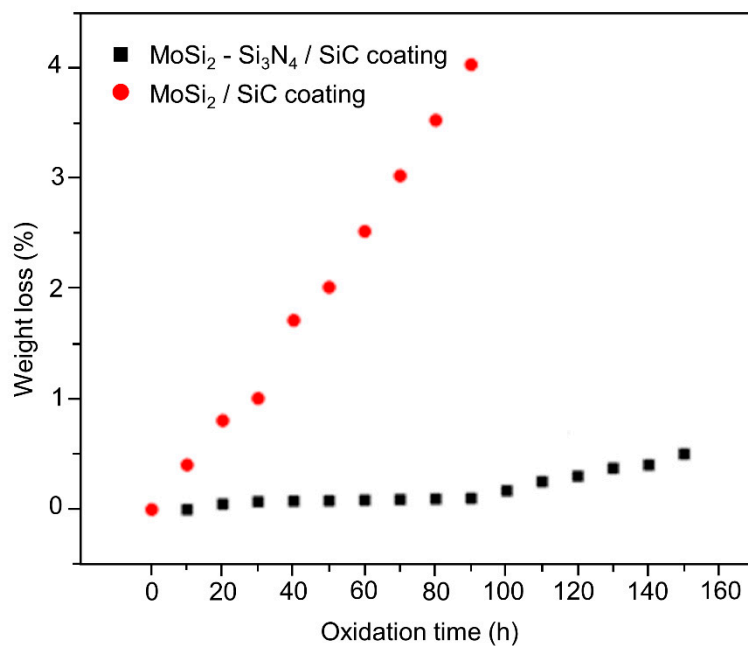
Figure 8. Isothermal oxidation curves of MoSi$_2$-Si$_3$N$_4$/SiC-coated C/C composites in the air at 1773 K.

The absence of Si_3N_4 in the $MoSi_2$/SiC coatings causes the pest disintegration of $MoSi_2$ which results in the coating's degradation at high temperatures. The increasing weight loss with oxidation time is due to the insufficient amount of SiO_2 that results in the formation of large cracks on the surface of the coating. This severely affects the coating surface and allows oxygen access to the C/C composites, causing gaseous byproducts. At high temperatures, these gaseous byproducts quickly evaporate to cause the sudden weight loss of the coating. This de-gasification produces some micro-cracks and deep cavities in the coating surface, which are the principal contributors to weight reduction.

The lower weight loss in the $MoSi_2$-Si_3N_4/SiC coating indicates that the addition of Si_3N_4 is beneficial for the coating's integrity at high temperatures. Additionally, the absence of debonding or spallation at 1773 K indicates that the Si_3N_4 in the coating yields better coating–substrate compatibility at high temperatures. This suggests that the $MoSi_2$-Si_3N_4 coating is more resistant to high-temperature oxidation.

3.3. Thermal Cyclic Oxidation Resistance of the Coating at 1773 K

Figure 9a shows the SEM image of the $MoSi_2$-Si_3N_4/SiC coating surface after the thermal cyclic oxidation test. It can be observed that whiskers are formed throughout the surface. The exposure of Si_3N_4 coatings to high temperatures can foster the formation of Si_2N_2O whiskers [33]. These whiskers play an essential role in increasing the oxidation resistance of the coating [34]. The cross-sectional view of the multi-layer coating in Figure 9b shows small pores, mainly caused by the rapid cooling from 1773 K to room temperature. These pores can be sealed by the formation of Si_3N_4 whiskers in the subsequent thermal cyclic oxidation process, which further protects the coating from high-temperature oxidation [35].
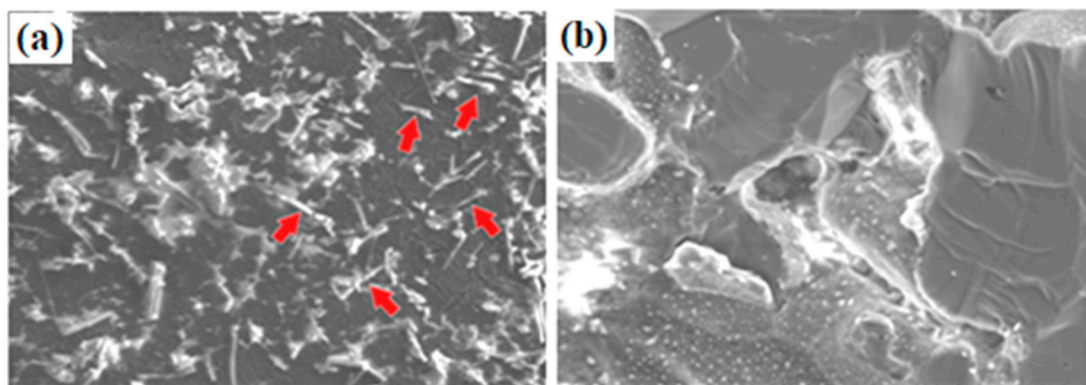
Figure 9. (**a**) Surface SEM image, where red arrows represent whiskers; (**b**) cross-section of multi-layer coatings after thermal cyclic oxidation test between 1773 K and room temperature 40 times.

Figure 10 shows the weight loss curve of the $MoSi_2$-Si_3N_4/SiC-coated C/C specimen during its repeated thermal cycling between 1773 K and room temperature. It can be observed that the weight loss of the coated specimen was only 0.05% after 40 thermal cycles. During the thermal cycling, the coating remained intact, and no oxidation or spallation was found. This indicates that the coating exhibits excellent oxidation and thermal cyclic oxidation resistance, which can be attributed to the filling of micro cracks under oxidizing environments by abundant glassy oxides.
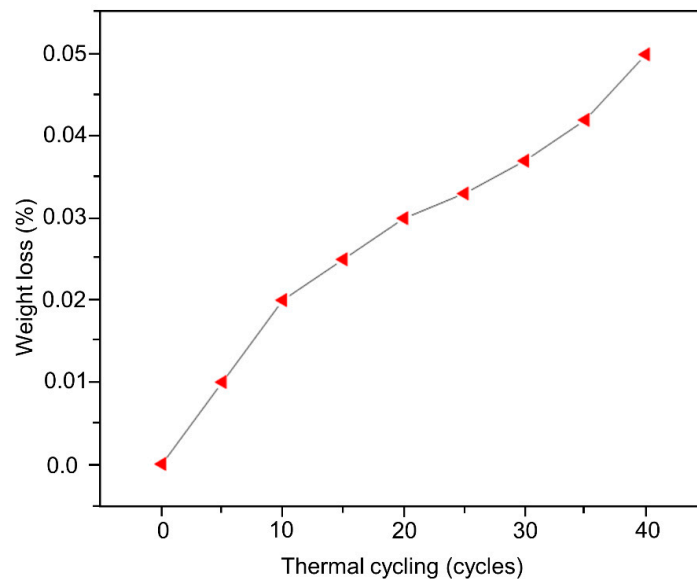
Figure 10. Thermal cycling oxidation curves of the MoSi$_2$-Si$_3$N$_4$/SiC coating between 1773 K and room temperature.

4. Conclusions

The effect of Si$_3$N$_4$ addition in MoSi$_2$/SiC coating on the oxidation and thermal cyclic oxidation resistance at 1773 K was investigated. The 0.5% weight loss in the MoSi$_2$-Si$_3$N$_4$/SiC coating after its oxidation for 150 h in comparison to the 4.0% weight loss in the MoSi$_2$/SiC coating after 90 h proves that the coating with Si$_3$N$_4$ has a better high-temperature oxidation resistance. The negligible weight loss after 40 thermal cycles between 1773 K and room temperature proves that the MoSi$_2$-Si$_3$N$_4$/SiC coating has an excellent thermal cyclic oxidation resistance. The presence of Si$_3$N$_4$ results in a complete transformation of MoSi$_2$ to SiO$_2$, which results in a dense glassy SiO$_2$ film. The SiO$_2$ film improves the coating's resistance to high-temperature oxidation by preventing gas diffusion into the coating, thus shielding the C/C substrate from byproduct-forming gases and delaying the generation of micro cracks. The addition of Si$_3$N$_4$ to the multi-layer coating is found to be beneficial for both coating integrity and coating–substrate compatibility.

References

1. Krenkel, W.; Berndt, F. C/C–SiC composites for space applications and advanced friction systems. *Mater. Sci. Eng. A* **2005**, *412*, 177–181. [CrossRef]
2. Katoh, Y.; Snead, L.L.; Henager, C.H., Jr.; Hasegawa, A.; Kohyama, A.; Riccardi, B.; Hegeman, H. Current status and critical issues for development of SiC composites for fusion applications. *J. Nucl. Mater.* **2007**, *367*, 659–671. [CrossRef]

3. Kim, B.G.; Dong, S.; Park, S.D. Effects of thermal processing on thermal expansion coefficient of a 50 vol.% SiCp/Al composite. *Mater. Chem. Phys.* **2001**, *72*, 42–47. [CrossRef]

4. Van der Berg, N.; Malherbe, J.B.; Botha, A.; Friedland, E. Thermal etching of SiC. *Appl. Surf. Sci.* **2012**, *258*, 5561–5566. [CrossRef]

5. Gasch, M.; Ellerby, D.; Irby, E.; Beckman, S.; Gusman, M.; Johnson, S. Processing, properties and arc jet oxidation of hafnium diboride/silicon carbide ultra high temperature ceramics. *J. Mater. Sci.* **2004**, *39*, 5925–5937. [CrossRef]

6. Kim, Y.-W.; Chun, Y.-S.; Nishimura, T.; Mitomo, M.; Lee, Y.-H. High-temperature strength of silicon carbide ceramics sintered with rare-earth oxide and aluminum nitride. *Acta Mater.* **2007**, *55*, 727–736. [CrossRef]

7. Fu, Q.-G.; Li, H.-J.; Shi, X.-H.; Li, K.-Z.; Sun, G.-D. Silicon carbide coating to protect carbon/carbon composites against oxidation. *Scr. Mater.* **2005**, *52*, 923–927. [CrossRef]

8. Zhang, Y.; Li, H.; Qiang, X.; Li, K. Oxidation protective C/SiC/Si-SiC multilayer coating for carbon/carbon composites applying at 1873 K. *J. Mater. Sci. Technol.* **2010**, *26*, 1139–1142. [CrossRef]

9. Chu, Y.; Li, H.; Fu, Q.; Wang, H.; Hou, X.; Zou, X.; Shang, G. Oxidation protection of C/C composites with a multilayer coating of SiC and Si+ SiC+ SiC nanowires. *Carbon* **2012**, *50*, 1280–1288. [CrossRef]

10. Tian, X.; Guo, X.; Sun, Z.; Qu, J.; Wang, L. Oxidation resistance comparison of $MoSi_2$ and B-modified $MoSi_2$ coatings on pure Mo prepared through pack cementation. *Mater. Corros.* **2015**, *66*, 681–687. [CrossRef]

11. Zhang, Y.-L.; Li, H.-J.; Qiang, X.-F.; Li, K.-Z.; Zhang, S.-Y. C/SiC/$MoSi_2$–Si multilayer coatings for carbon/carbon composites for protection against oxidation. *Corros. Sci.* **2011**, *53*, 3840–3844. [CrossRef]

12. Fu, Q.; Shan, Y.; Cao, C.; Li, H.; Li, K. Oxidation and erosion resistant property of SiC/Si–Mo–Cr/$MoSi_2$ multi-layer coated C/C composites. *Ceram. Int.* **2015**, *41*, 4101–4107. [CrossRef]

13. Feng, T.; Li, H.-J.; Fu, Q.-G.; Shen, X.-T.; Wu, H. Microstructure and oxidation of multi-layer $MoSi_2$–$CrSi_2$–Si coatings for SiC coated carbon/carbon composites. *Corros. Sci.* **2010**, *52*, 3011–3017. [CrossRef]

14. Friedrich, C.; Gadow, R.; Speicher, M. Protective multilayer coatings for carbon–carbon composites. *Surf. Coat. Technol.* **2002**, *151*, 405–411. [CrossRef]

15. Wu, H.; Li, H.-J.; Ma, C.; Fu, Q.-G.; Wang, Y.-J.; Wei, J.-f.; Tao, J. $MoSi_2$-based oxidation protective coatings for SiC-coated carbon/carbon composites prepared by supersonic plasma spraying. *J. Eur. Ceram. Soc.* **2010**, *30*, 3267–3270. [CrossRef]

16. Shi, X.; Wang, C.; Lin, H.; Huo, C.; Jin, X.; Shi, G.; Dong, K. Oxidation resistance of a La–Mo–Si–O–C coating prepared by supersonic atmosphere plasma spraying on the surface of SiC-coated C/C composites. *Surf. Coat. Technol.* **2016**, *300*, 10–18. [CrossRef]

17. Li, H.-J.; Xue, H.; Wang, Y.-J.; Fu, Q.-G.; Yao, D.-J. A $MoSi_2$–SiC–Si oxidation protective coating for carbon/carbon composites. *Surf. Coat. Technol.* **2007**, *201*, 9444–9447. [CrossRef]

18. Fu, Q.; Zou, X.; Chu, Y.; Li, H.; Zou, J.; Gu, C. A multilayer $MoSi_2$–SiC–B coating to protect SiC-coated carbon/carbon composites against oxidation. *Vacuum* **2012**, *86*, 1960–1963. [CrossRef]

19. Feng, T.; Li, H.; Shi, X.; Yang, X.; Wang, S.; He, Z. Multi-layer CVD-SiC/$MoSi_2$–$CrSi_2$–Si/B-modified SiC oxidation protective coating for carbon/carbon composites. *Vacuum* **2013**, *96*, 52–58. [CrossRef]

20. Zhang, H.; Lv, J.; Zhuang, S.; Chen, Y.; Gu, S. Effect of WSi_2 and Si_3N_4 contents on the thermal expansion behaviors of (Mo, W) Si_2-Si_3N_4 composites. *Ceram. Int.* **2017**, *43*, 2847–2852. [CrossRef]

21. Li, L.; Li, H.; Shen, Q.; Lin, H.; Feng, T.; Yao, X.; Fu, Q. Oxidation behavior and microstructure evolution of SiC-ZrB_2-ZrC coating for C/C composites at 1673 K. *Ceram. Int.* **2016**, *42*, 13041–13046. [CrossRef]

22. He, Z.; Li, H.; Shi, X.; Fu, Q.; Wu, H. Microstructure and oxidation resistance of SiC–$MoSi_2$ multi-phase coating for SiC coated C/C composites. *Prog. Nat. Sci. Mater. Int.* **2014**, *24*, 247–252. [CrossRef]

23. Huang, Y.; Lin, J.; Zhang, H. Effect of Si_3N_4 content on microstructures and antioxidant properties of $MoSi_2$/Si_3N_4 composite coatings on Mo substrate. *Ceram. Int.* **2015**, *41*, 13903–13907. [CrossRef]

24. Hu, M.; Li, K.; Wang, J. Effect of Cr content on the microstructure and thermal properties of $ZrSi_2$–$CrSi_2$–SiC multiphase coating for the SiC coated C/C composites. *Ceram. Int.* **2016**, *42*, 19357–19364. [CrossRef]

25. Srivastava, A.; Tripathi, P.; Nayak, M.; Lodha, G.; Nandedkar, R. Formation of Mo_5Si_3 phase in Mo/Si multilayers. *J. Appl. Phys.* **2002**, *92*, 5119–5126. [CrossRef]

26. Fabrizi, A.; Cecchini, R.; Kiryukhantsev-Korneev, P.V.; Sheveyko, A.N.; Spigarelli, S.; Cabibbo, M. Comparative investigation of oxidation resistance and thermal stability of nano-structured Ti-B-N and Ti-Si-B-N coatings. *J. Prot. Met. Phys. Chem. Surf.* **2017**, *53*, 452–459. [CrossRef]

27. Jianhui, Y.; Hongmei, X.U.; Houan, Z.; Siwen, T. MoSi$_2$ oxidation resistance coatings for Mo$_5$Si$_3$/MoSi$_2$ composites. *Rare Met.* **2009**, *28*, 418–422.

28. Fu, Q.-G.; Jing, J.-Y.; Tan, B.-Y.; Yuan, R.-M.; Zhuang, L.; Li, L. Nanowire-toughened transition layer to improve the oxidation resistance of SiC–MoSi$_2$–ZrB$_2$ coating for C/C composites. *Corros. Sci.* **2016**, *111*, 259–266. [CrossRef]

29. Huang, J.-F.; Wang, B.; Li, H.-J.; Liu, M.; Cao, L.-Y.; Yao, C.-Y. A MoSi$_2$/SiC oxidation protective coating for carbon/carbon composites. *Corros. Sci.* **2011**, *53*, 834–839. [CrossRef]

30. Iizuka, T.; Kita, H. Tribological behavior of Mo$_5$Si$_3$ particle reinforced Si$_3$N$_4$ matrix composites. *Wear* **2005**, *258*, 877–889. [CrossRef]

31. Zhang, J.; Fu, Q.; Qu, J. Enhanced bonding strength and thermal cycling performance of MoSi$_2$–CrSi$_2$–SiC–Si coating for carbon/carbon composites by surface modification via blasting treatment. *Ceram. Int.* **2016**, *42*, 14021–14027. [CrossRef]

32. Yoon, J.-K.; Lee, K.-H.; Kim, G.-H.; Han, J.-H.; Doh, J.-M.; Hong, K.-T. Low-temperature cyclic oxidation behavior of MoSi$_2$/SiC nanocomposite coating formed on Mo substrate. *Mater. Trans.* **2004**, *45*, 2435–2442. [CrossRef]

33. De la Pena, J.; Pech-Canul, M. Microstructure and kinetics of formation of Si$_2$N$_2$O and Si$_3$N$_4$ into Si porous preforms by chemical vapor infiltration (CVI). *Ceram. Int.* **2007**, *33*, 1349–1356. [CrossRef]

34. ZhongLiu, W.; Peng, X.; Zhuan, L.; XiaoYu, Y.; Yang, L. Thermal cycling behavior and oxidation resistance of SiC whisker-toughened-mullite/SiC coated carbon/carbon composites in burner rig tests. *Corros. Sci.* **2016**, *106*, 179–187. [CrossRef]

35. Lai, Z.; Meng, S.; Zhu, J.; Jeon, J. Microstructure of a Mo-Si-CN multi-layered anti-oxidation coating on carbon/carbon composites by fused slurry. *Rare Met.* **2009**, *28*, 460–464. [CrossRef]